WES-2025-283: Reply to Referee 2

Referee: " This paper presents a thorough and detailed explanation of an improved analytical model for flow curvature corrections of lift, drag, and moment coefficients for reduced-order modeling of cross-flow turbines. Detailed equations, as well as the approximations made, are presented in the body of the paper and supported in several appendices.

Reply: we thank the referee for his positive global appreciation of our contribution to the simulation, using ALM, of flows with curvature effects such as those in vertical-axis turbines (VATs, for wind or water); also called cross-flow turbines. The study is indeed extensive and general, and the proposed methodology is shown to be very effective at predicting the time-evolution, over one blade revolution, of the loads (forces and moment). We put much effort in validating the proposed models against high-quality wall-resolved simulations of the fictitious single-blade VAT (previously studied by T. Villeneuve et al., by the U. Laval group), and for different locations of the blade attachment point.

Referee: "Technical comments:"

Reply: We answer below to the points by points comments/requests, and we modify the paper accordingly.

Referee: "- Lines 27 and 28 mention that high-fidelity numerical simulations are a precise approach for modeling cross-flow turbines, and CFD simulations are used later on for validation. However, CFD can still produce significant errors when modeling the unsteady dynamics of cross-flow turbines. Whether or not the CFD used for validation has been compared to experimental results should be addressed."

Reply: The CFD methodology consists in high quality wall-resolved RANS (steady) and URANS (unsteady) simulations. The RANS approach is used in conjunction with the Spalart-Allmaras turbulence closure model, which is recognized as a good model for external flow aerodynamics past airfoils. We here also use, on purpose, a high Reynolds number of $Re_c = 6.0 \times 10^6$ so that the boundary layers are fully turbulent, which further validates the use of RANS.

The present RANS simulation setup has also been validated in 3D, against experimental data of the pressure coefficient distribution along the airfoil chord at different spanwise location of a 3D wing (up to near the tip) by Chow et al. (J.S. Chow, G.G. Zilliac, P. Bradshaw, Turbulence measurements in the near field of a wingtip vortex, in: Tech. Rep. NASA-TM-110418, 1997). At $z/b = 0.362$, the numerical curve and the experimental data are almost superimposed along the entire chord length of the wing. At $z/b = 0.906$ and $z/b = 0.966$, there are small differences on the wing suction side near the trailing edge, but globally, the numerical curves match the experimental data very well. This validation is also reported in Figure 5 of Villeneuve et al (2021). The reference simulations, and models, in the present paper being for 2D airfoils, we are very confident in the quality of our RANS results. We have added the following sentence at the begining of Appendix A:

"We note that the simulation setup has also been validated against experimental data of the pressure coefficient distribution along the airfoil chord, at different spanwise location of a 3D wing, and up to near the wing tip; this is reported in Villeneuve et al. (2021)."

Last, but not least: Our modeling approach is self-consistent whatever the reference CFD data. Indeed: the reference aeodynamic coefficients for the airfoil in uniform flow, as a function of the angle of attack, are obtained using our RANS simulation setup (see Appendix A), and it is those coefficients that are then used, together with our modeling for the flow curvature corrections. The reference data for the rotating airfoil with $c/R = 2/7$ are then also obtained using our RANS simulation setup, and for the two cases of attachment point, $x_p = c/2$ and $x_p = c/4$ (see Appendix B); and we then show in the core of the paper that our correction models, that use the aerodynamic coefficients obtained in Appendix A, are indeed able to duplicate those data quite well: see Section 3.3.4 for the case with $x_p = c/2$ and Section 3.4.1 for the case with $x_p = c/4$).

If we changed the simulation setup, we would obtain different "reference aerodynamic coefficients" in Appendix A; and we would use those, together with our models for curvature corrections, and then duplicate the results of the rotating airfoil also obtained using the changed simulation setup. Hence the self-consistency of the approach that we used.

Concerning unsteady flows: For the URANS of the VAT configuration, we used the $TSR = 3.5$ value because it is high enough that the flow past the blade does not separate dynamically at any position on the cycle. Hence, although the flow is unsteady, the boundary layers remain attached and they are no dynamic stall effects. Here too: the simulations using ALM and combined with our flow correction models, that use gain aerodynamic coefficients of Appendix A, are self-consistent with our reference RANS simulation setup.

Please also recall that, when an ALM is used for an unsteady flow, vorticity is continuously shed into the wake, as it should; hence, the Biot-Savart velocity induced by this wake vorticity is properly taken into account when we measure the effective velocity (see Section 4 and Figure 13)

In fact, it is because we know, from previous wall-resolved simulations of the present single-blade fictitious VAT by T. Villeneuve, who performed simulations that span the full range of TSR values for his PhD thesis, that $TSR = 3.5$ corresponds to the case of maximum power production AND without significant boundary layer separation. We have added the following at the beginning of Section 6:

"This value is also high enough that the flow past the blade does not separate dynamically at any position over the cycle; as is confirmed when examining the vorticity field of the wall-resolved simulation in Figure 13. Hence, using the static airfoil polar data, solely corrected for flow curvature effects (i.e. no added dynamic polar model), is expected to be sufficient."

Concerning the details of the URANS simulation setups: we have also revisited Section 6 concerning the VAT configuration case, following a request by the other Referee.

Added note for lower TSR: For significantly lower TSR values, say $TSR = 2.5$, the span of angles of attack seen by the blade over the cycle becomes larger, and it would become necessary to also include unsteady corrections to model the dynamic effects on the polar (even possibly dynamic stall effects); for instance using the Leishman and Beddoes dynamic airfoil

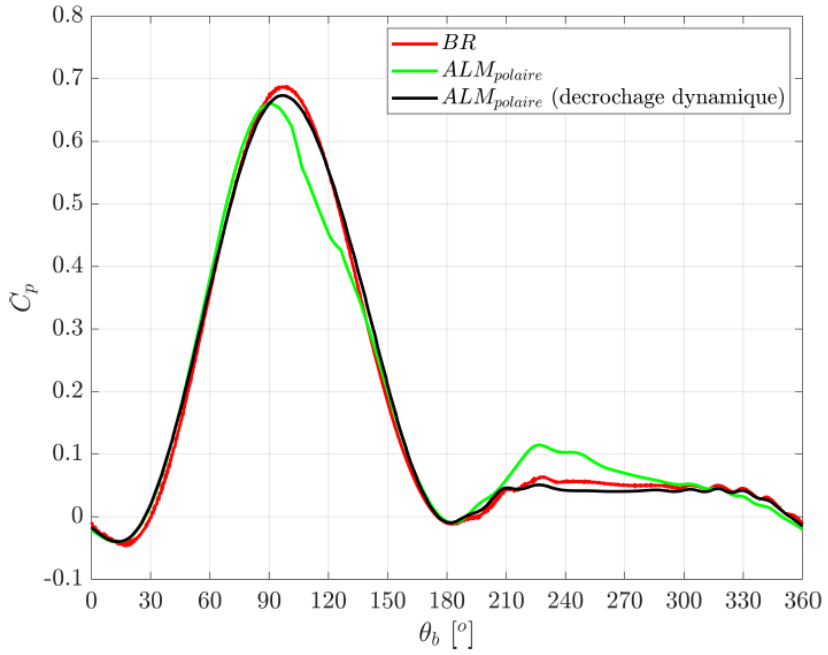

Figure 1: Illustrative results of ALM simulations for the case of a VAT configuration with $R/c = 6$ operating at $TSR = 2.5$; courtesy of P. Rochefort and M. Mordret. Power coefficient for the reference wall-resolved CFD (red), for the ALM using the static airfoil polar model and the corrections for flow curvature effects (green), ALM using a dynamic model for the aifoil polar and the corrections for flow curvature effects (black).

polar model, or the quasi-steady theory of Theodorson, or the model of Viterna to extrapolate the polars. For instance, P. Rochefort did a study with a stagiaire (M. Mordret) of a VAT configuration with $R/c = 6$ operating at $TSR = 2.5$: some results are shown in Figure 1 of this reply document, in confidence. It is seen that a dynamic model for the airfoil polar is indeed required in addition to the corrections for flow curvature effects; and it is also seen that combining both produces results that compare quite well with those of the reference wall-resolved CFD.

Referee: "- Line 87: It is not clear which 2 stall angles are being referred to.

Reply: The stall angles of a symmetric airfoil, such as the NACA0015 used here, are indeed different for positive pitch and negative pitch, due to flow curvature effects. For the case with $x_p = c/2$, they are measured, in the reference RANS simulations as -19 deg and 17 deg: see Section 3.3.4. For the case with $x_p = c/4$, they are measured as ?16 deg and 20?21 deg: see Section 3.4.1. We have made the sentence more clear:

"... and here up to the two stall angles (i.e., those for negative pitch and positive pitch, which are indeed different due to flow curvature)."

Referee: "- Lines 114-115: It would be helpful to show the normal forces being referred to here on the figure to illustrate the force directions being described

Reply: Please note that arrows showing the normal and tangential forces are clearly shown in Figures 2, 3 and 5. We don't want to mess up Figure 1, that shows nice streamlines of the potential flow, with added arrows. Instead, we improved the text to make it more clear:

"The case with $\alpha_p = 0$ corresponds to a flow that is left/right symmetric; the normal force exerted by the flow on the plate acts downward. The case with $\alpha_p = 4$ deg has a normal force close to zero. The case with $\alpha_p = 8$ deg has a normal force acting upward."

Referee: "- Line 118: Clarify why the circulation is set as negative"

Reply: The circulation of a vortex in the $x - y$ plane is defined positive when it is anti-clockwise (i.e., when the flow direction that it induces goes from the x axis to the y axis. It is thus set negative here because the vortex is below the plate and that it induces on the plate a flow that goes from left to right; as in the Figures 1, 2, 3 and 5. Note also that the same convention is used for obtaining the exact solution of the potential flow in Appendix E.

Referee: "- Equation 1: Clarify or introduce the "z" variable

Reply: The potential flow induced by the vortex is here obtained using the complex variable $z = x + i\,y$, and the complex potential is $\phi + i\,\psi$, with ϕ the potential (i.e., $u = \frac{\partial \phi}{\partial x}$ and $v = \frac{\partial \phi}{\partial y}$) and ψ the streamfunction (i.e., $u = \frac{\partial \psi}{\partial y}$ and $v = -\frac{\partial \psi}{\partial x}$). We have improve the paper as follows:

"The complex potential due to the vortex is

$$f(z) = \phi(z) + i\,\psi(z) = -i\,\frac{\Gamma_0}{2\pi}\,\log\left(\frac{z + i\,R}{R}\right) = i\,U\,R\,\log\left(\frac{z}{R} + i\right) \tag{1}$$

with $z = x + i\,y$ the complex variable, $\phi(z)$ the potential and $\psi(z)$ the streamfunction.

Referee: "- Figures 4 and 6: Clarify or explain the significantly larger error in the $C_{m_{c/4}}$ plots

Reply: The model for the moment $C_{m_{c/4}}$ was clearly explained in the paper: it is based on the usual inviscid potential flow for an arfoil with camber (shown in Figure 2, (b) and (c)), and hence is solely valid for moderate pitch angles: see lines 229 to 235 and Eq. (16) for the case with $x_p = c/2$.

The discussion about the results, and the importance of $C_{m_{c/2}}$ at zero pitch angle (which is zero for the flat plate, by symmetry; but non zero for the airfoil in rotation) was done in details on lines 265 to 272. When using the modeled value of $C_{m_{c/2}}$ (as obtained in Appendix C), the model prediction at zero pitch angle is $C_{m_{c/4}} = 0.1079$: this compares very well with $C_{m_{c/4}} = 0.10225$ for the reference CFD, as shown in Figure 4 (5.5% error). This is indeed twice better than when neglecting to also model $C_{m_{c/2}}$ (i.e., assuming that it is zero, as for the flat plate), leading to a prediction of $C_{m_{c/4}} = 0.1135$ (11% error). It is thus important

to also take into account a model for $C_{m_{c/2}}$, and this too constitutes a contribution of our paper.

Now: it must be recognized that a simple model for $C_{m_{c/4}}$ is based on the analogy with that of the inviscid potential flow theory for a cambered airfoil: Eq. (16). As such, it cannot take into account deviations when at pitch angles exceeding 10 deg, where the viscous effects on the moment also become significant (even when the boundary layers remain attached, as is the case here before stall). This is a known fact for any real airfoil in a viscous flow; even for airfoils without camber. For instance, if you consider the NACA0012 airfoil in a uniform flow, one measures that $C_{m_{c/4}} = 0$ for small angles (as it should since no camber), but this is no longer valid when one exceeds 10 deg (with $C_{m_{c/4}} \simeq -0.2$ when at 16 deg). We have thus improved the paper and added this at the end of Section 3.3.4, when discussing the results:

"Finally, we stress that the model for $C_{m_{c/4}}$ is based on the analogy with that of the inviscid potential flow for a cambered airfoil. As such, it cannot take into account deviations from that when the pitch angle exceeds $\simeq 10$ deg, where viscous effects on the moment also become significant; and leading to deviations up to $\simeq 0.025 - 0.03$ near stall."

Concerning Figure 6: the same type of model as for $x_p = c/2$ is used for the case with $x_p = c/4$, see lines 325 to 328 with Eq. (33); leading to the same type of result in Figure 6, withnthe same good value ar zero pitch, and the same problems at high pitch angle.

Referee: "Typographical comments'
- Line 9: "inviscid part correspond to" should be "inviscid part corresponds to"
- Line 84: Missing a space in "Section3".
- Figure 1: Font sizes on axes should be larger
- Figure 5: Caption refers to plot (c) when there is no such plot shown
- Line 416: "Here, We use" should be "Here, we use"
- Line 662: "various pitch angles and for angle up to stall" should be "various pitch angles and for angles up to stall"

Reply: Thank you very much for finding those ! We have corrected them.